PERGAMON

International Journal of Solids and Structures 38 (2001) 6381–6403

INTERNATIONAL JOURNAL OF SOLIDS and STRUCTURES

www.elsevier.com/locate/ijsolstr

Static shape control of composite plates using a curvature–displacement based algorithm

C. Chee, L. Tong *, G.P. Steven

School of Aerospace, Mechanical and Mechatronic Engineering, University of Sydney, Building J07, Sydney 2006, NSW, Australia

Received 2 August 2000

Abstract

An intuitive algorithm for the determination of voltage distribution in the application to shape control of smart structures using piezoelectric actuators is presented here. This approach uses curvature as the fine-tuning criteria on top of the common displacement-based shape control, and is an extension of the slope–displacement method developed by the same authors. The algorithm called the perturbation buildup voltage distribution (PBVD) is based on an iterative approach inspired by a previous algorithm BVD on displacement control. This method aims to provide a means of targeting the desired shape of a structure by using a higher level shape attribute, in this case curvature. Intuitive iterative parameters of the PBVD method allow the user to have better control over the degree of conformity of the structure's shape. A natural consequence of this method is the smoothing of the resultant shape. Results show that the slopes and curvatures of the structure can be improved but at a tolerable expense of the displacement criteria. Another result of practical interest is the reduction of internal stresses compared to cases using pure displacement shape control.

Keywords: Curvature; Shape control; Finite element; Perturbation; Composite; Piezoelectric; Layerwise; High order displacement

1. Introduction

Significant interest has been raised in the field of smart or intelligent structures, over the past decade. Conventional structural engineering usually involves structures which are passive but the new technology of smart structures involve active structures, that is, structures with the ability to change its overall properties or configuration while in operation. The smartness or the intelligence of the structure refers to the ability of the structure to actuate itself using some built-in control algorithms to actuate the adaptive materials incorporated in the structure. It may depend on the response obtained by a set of sensors also made of adaptive materials. Such a self-contained system has the ability to perform various tasks such as vibration control, shape control, health monitoring and stability control.

* Corresponding author. Tel.: +61-2-9351-6949; fax: +61-2-9351-4841.
E-mail address: ltong@aero.usyd.edu.au (L. Tong).

0020-7683/01/$ - see front matter
PII: S0020-7683(01)00049-X

Nomenclature

BVD	buildup voltage distribution
CDSC	curvature displacement shape control
CPI	curvature patch insensitivity index
DBSC	displacement based shape control
LLS	linear least squares
LS	least squares
McLLS	multi-criteria linear least squares
MCSC	multi-criteria shape control
PBVD	perturbation buildup voltage distribution
SDSC	slope–displacement shape control

Shape control applications had existed before the concept of smart structures in particular regarding the shape control of space antenna, reflectors etc., (Haftka and Adelman, 1985). Many such work involving space truss structures are based on controlling the shape at discrete points using conventional axial (point) actuators. The application considered in this paper is that of quasi-static shape control. Shape control involves manipulating the structure's shape to conform to a desired shape specified by the user. Applications range from controlling the shape of aerodynamic surfaces such as an aerofoil to large flexible space structures (Okubo et al., 1996) or space antenna reflectors (Tabata and Natori, 1996). It has been noted that smart actuators integrated within the structure produces small in-plane deflections that can in turn produce large out-of-plane deformations (Paradies et al., 1996). The objective of shape control is to obtain a shape that is as close as possible to the desired shape by either determining the magnitude of input signal to apply to each actuator, or the optimal layout of actuators, as well as determining any other variables that might affect the behavior of the structure. Several works presented results of various shapes obtained by changing input parameters such as actuator size, location and actuator voltages (Donthireddy and Chandrashekhara, 1996; Eisenberger and Abramovich, 1997). Although the viability of the shape control of structures was shown, they did not address the shape control problem directly.

The true shape control problem is a type of inverse problem with no explicit solutions. The core of shape control is to minimize the cost functional usually defined as the squared difference of displacements between the desired and the calculated/actual shape. Koconis et al. (1994a,b) developed analytical methods for composite plates and shells based on sandwich structures and finding solutions to expressions corresponding to zero slope with respect to variables to be optimized. Hsu et al. (1997) adopted finite elements for composite plates and used a "gradient projection method" to find the "search direction". Until now most plate models have been based on Kirchoff's thin plate theory or the first order shear deformation theory; there has been little work on shape control using high order displacement theories for composite plates.

An iterative approach for shape control of composite beams was formulated by Chandrashekhara and Varadarajan (1997) using Reddy's (1984) third order displacement theory while the composite plate version (Varadarajan et al., 1998) used first order shear deformation theory. Besides minimizing the error function, they also considered closed loop control where the displacements are fed back to determine the next set of input voltages. Techniques of using optimal linear quadratic Gaussian for shape control of smart structures were implemented by Balakrishnan (1994) and Tan and Bainum (1994a,b). Alternatively, there are simpler heuristic methods that have been developed for general shape control of structures which are not necessarily smart structures. Some of these are the Worst-in-Best-out and the exhaustive single point substitution

and Skelton and DeLorenzo's (SD) method (see Haftka and Adelman, 1985). The latter algorithm is based on choosing all actuators initially and then removing those which make the least contribution. Another method called the successive peak error correction (SPEC) (Subramanian and Mohan, 1996) was claimed to be faster than the SD method but with comparable precision.

In Chee et al. (2000b), an intuitive/heuristic shape control algorithm was developed that has been inspired by elements of the SPEC method, evolutionary strategies and artificial neural networks. The algorithm called BVD, iteratively builds up the voltage magnitudes of each potentially active patch, thus resulting in a final voltage distribution. Like many other shape control work, BVD is solely displacement based. Following this, Chee et al. (2000c) introduced slope as the next criteria for shape control. Thus a dual-criteria SDSC algorithm, called PBVD, was developed. PBVD is an iterative algorithm with a concept similar to BVD. Initially displacement shape control based on a LLS fit is performed on the structure. The result is a structure with some bumpiness and this is taken as the initial configuration for PBVD.

The work presented in this paper extends the concept of MCSC to include curvatures as the additional criteria, instead of slopes. Thus in PBVD, curvature is regarded as the fine-tuning criteria to smoothen the structure. In the iterative process, the voltages are perturbed and build up based on a cost function determined by the curvature. Unlike the least square method, PBVD makes no assumption on linearity and hence can be used for general non-linear piezo-elastic systems. Initial investigation includes dual criteria CDSC using standard McLLS. It will be shown that due to the competing effects of displacement and curvature, it is very difficult to select the parameters of McLLS. In comparison, the PBVD parameters are more intuitive. The results will show that the smoothing of transverse displacement achieved by PBVD–SDSC (Chee et al., 2000c) will also be achieved here by PBVD–CDSC. In addition, there is greater reduction in stresses achieved here.

2. Mathematical model

The present work will consider a composite laminate plate structure as the smart structure using piezoelectric materials as the adaptive actuators. The mathematical model is a hybrid of a high (third) order displacement theory and layerwise concept (Chee et al., 2000a) that fully accounts for the electromechanical coupling. This also allow both thin and thick composite structures to be modeled and the piezoelectric actuators can be placed in any of the layers (i.e. embedded or surface bonded). The model is then incorporated into a finite element (FE) formulation which, in general, also accommodates greater freedom as to where the actuators may be placed. The use of finite element analysis (FEA) mean that the geometry is not restricted to simple shapes unlike that required by exact analytical solutions methodologies. The FEA calculations will be done using an in-house developed program based on the theoretical formulation.

2.1. Governing equations

The mechanical behavior of the structure is modeled by the third order displacement field, used by Lo et al. (1977), as shown in Eq. (1).

$$\begin{aligned} U(x,y,z) &= u_0(x,y) + z\psi_x(x,y) + z^2\zeta_x(x,y) + z^3\phi_x(x,y) \\ V(x,y,z) &= v_0(x,y) + z\psi_y(x,y) + z^2\zeta_y(x,y) + z^3\phi_y(x,y) \\ W(x,y,z) &= w_0(x,y) + z\psi_z(x,y) + z^2\zeta_z(x,y) \end{aligned} \tag{1}$$

The displacement functions U, V, W in the x, y, z directions, are composed of in-plane sub-functions such as $u_0(x,y)$, $v_0(x,y)$, $w_0(x,y),\ldots,\phi_y(x,y)$, etc., which are separated from the thickness (z) dimension. The advantages of the cubic HOD are (i) It is suitable for both thick and thin composite structures. (ii) No

shear correction factor is required. (iii) Models the transverse shear effects and captures a parabolic transverse shear strain across the thickness of the structure. (iv) Transverse normal strain is also accounted for. (v) Less restriction on the type of problem because displacement field is independent of boundary conditions and material properties. (vi) The absence of derivatives in the displacement field means that C^0 shape functions can be used in the FE formulation. This represents a total of 11 mechanical degrees of freedom (Eq. (2)).

$$u = [\, u_0 \quad v_0 \quad w_0 \quad \psi_x \quad \psi_y \quad \psi_z \quad \zeta_x \quad \zeta_y \quad \zeta_z \quad \phi_x \quad \phi_y \,]^{\mathrm{T}} \tag{2}$$

The strain vector Eq. (3), are defined in the usual manner and thus will not be elaborated further.

$$[\, \varepsilon_1 \quad \varepsilon_2 \quad \varepsilon_3 \quad \varepsilon_6 \,]^{\mathrm{T}} = \varepsilon_b = D_b u$$

$$[\, \varepsilon_4 \quad \varepsilon_5 \,]^{\mathrm{T}} = \varepsilon_s = D_s u \tag{3}$$

The linear layerwise formulation has been used by Saravanos and Heyliger (1995), and before them, Robbins and Reddy (1991). This technique will be applied to the electric potential and separates the field into planar (ϕ_j) and transverse layerwise (L_j) functions. General layerwise function may be written as Eq. (4).

$$\Phi(x,y,z,t) = \sum_{j=1}^{n\text{layers}+1} L_j(z)\phi_j(x,y,t) \tag{4}$$

The structure is divided into several layers, and each layer can be approximated by a *linear* electric potential field in the z direction. Hence if the overall electric potential across the thickness is a polynomial function of n-degree, then there should be at least n discrete layers for this layerwise approximation. So the electric potential within the kth layer is given in Eq. (5).

$$\Phi(x,y,z)_k = L_{kd}(z)\phi_k(x,y) + L_{ku}(z)\phi_{k+1}(x,y) \quad \text{where } L_{kd}(z) = \frac{z - z_{k+1}}{z_k - z_{k+1}}, \quad L_{ku}(z) = \frac{z - z_k}{z_{k+1} - z_k} \tag{5}$$

Note that $\phi_k(x,y)$ and $\phi_{k+1}(x,y)$, are functions at the kth and $(k+1)$th interfaces respectively.

From definition of the electric field being the negative gradient of the electric potential, the layerwise expression for the electric field at the kth layer is Eq. (6).

$$\begin{bmatrix} E_x(x,y,z) \\ E_y(x,y,z) \\ E_z(x,y,z) \end{bmatrix}_k = -\begin{bmatrix} L_{kd}(z)\frac{\partial\phi_k(x,y)}{\partial x} + L_{ku}(z)\frac{\partial\phi_{k+1}(x,y)}{\partial x} \\ L_{kd}(z)\frac{\partial\phi_k(x,y)}{\partial y} + L_{ku}(z)\frac{\partial\phi_{k+1}(x,y)}{\partial y} \\ \frac{1}{z_k - z_{k+1}}\phi_k(x,y) + \frac{1}{z_{k+1} - z_k}\phi_{k+1}(x,y) \end{bmatrix} \tag{6}$$

The FE formulation is based on the Hamilton's variational principle which considers the strain potential energy and work for the whole structure. Thus, the mechanical behavior modeled by the HOD theory and the electrical behavior modeled by the layerwise theory will be fully coupled. The natural boundary conditions are also implicitly accounted for. The present work will neglect the kinetic energy term.

The potential energy is the internal potential strain energy of the system or structure. And for piezoelectric systems, i.e. structures which have parts that are piezoelectric materials, the potential energy (Tiersten, 1969) is stated in Eq. (7):

$$\mathrm{d}P = (\sigma\,\mathrm{d}\varepsilon - D\,\mathrm{d}E) \times \text{Volume} \tag{7}$$

The specific form of potential energy (P) of Eq. (7) was chosen because its natural variables are strain (ε) and electric field (E), both of which can be expressed in terms of displacement and electric voltage respectively, which are obvious choices as degrees of freedom in FEA. This necessitates the use of the stress formulation of the piezoelectric constitutive equation as shown in Eqs. (8a) and (8b).

$$\begin{pmatrix}\sigma_1\\ \sigma_2\\ \sigma_3\\ \sigma_6\end{pmatrix} = \begin{bmatrix} c_{11} & c_{12} & c_{13} & c_{16}\\ c_{12} & c_{22} & c_{23} & c_{26}\\ c_{13} & c_{23} & c_{33} & c_{36}\\ c_{16} & c_{26} & c_{36} & c_{66}\end{bmatrix}\begin{pmatrix}\varepsilon_1\\ \varepsilon_2\\ \varepsilon_3\\ \varepsilon_6\end{pmatrix} - \begin{pmatrix} e_{31}\\ e_{32}\\ e_{33}\\ e_{36}\end{pmatrix} E_3,$$
$$\begin{pmatrix}\sigma_4\\ \sigma_5\end{pmatrix} = \begin{bmatrix} c_{44} & c_{45}\\ c_{45} & c_{55}\end{bmatrix}\begin{pmatrix}\varepsilon_4\\ \varepsilon_5\end{pmatrix} - \begin{bmatrix} e_{14} & e_{24}\\ e_{15} & e_{14}\end{bmatrix}\begin{pmatrix}E_1\\ E_2\end{pmatrix} \tag{8a}$$

$$\sigma_b = c_b\varepsilon_b - e_b^{\mathrm{T}}E_0, \quad \sigma_s = c_s\varepsilon_s - e_s^{\mathrm{T}}E_i$$

$$\begin{pmatrix}D_1\\ D_2\end{pmatrix} = \begin{bmatrix} e_{14} & e_{15}\\ e_{24} & e_{14}\end{bmatrix}\begin{pmatrix}\varepsilon_4\\ \varepsilon_5\end{pmatrix} + \begin{bmatrix}\chi_{11} & \chi_{12}\\ \chi_{12} & \chi_{22}\end{bmatrix}\begin{pmatrix}E_1\\ E_2\end{pmatrix}, \quad D_3 = [\,e_{31} \quad e_{32} \quad e_{33} \quad e_{36}\,]\varepsilon_b + \chi_{33}E_3 \tag{8b}$$

$$D_i = e_s\varepsilon_s + \chi_i E_i, \qquad D_0 = e_b\varepsilon_b + \chi_0 E_0$$

The substrate material is orthotropic at most and the piezoelectric material is "orthorhombic-class mm2" as indicated by Eqs. (8a) and (8b). Piezoelectric stress coefficients (e_b and e_s) are set to zero for non-piezoelectric materials. The global coordinate system used in Eqs. (8a) and (8b) has taken into account the rotation of the material about the transverse normal z-axis. For a material with zero rotation, then the following material coefficients are zero: c_{16}, c_{26}, c_{36}, c_{45}, e_{14}, e_{36}, χ_{12}.

Using the constitutive Eqs. (8a) and (8b), the potential energy integral can be expressed in terms of virtual strains and electric fields as:

$$\delta\int_{t_1}^{t_2} P\,\mathrm{d}t = \int_{t_1}^{t_2}\int_V \{\delta\varepsilon_b^{\mathrm{T}}(c_b\varepsilon_b - e_b^{\mathrm{T}}E_0) + \delta\varepsilon_s^{\mathrm{T}}(c_s\varepsilon_s - e_s^{\mathrm{T}}E_i) - \delta E_i^{\mathrm{T}}(e_s\varepsilon_s + \chi_i E_i) - \delta E_0^{\mathrm{T}}(e_b\varepsilon_b + \chi_0 E_0)\}\,\mathrm{d}V\,\mathrm{d}t \tag{9}$$

The total virtual work of a structure is generally due to the mechanical forces including volume, surface forces and point forces acting on displacements and also due to electrical charges in the presence of an electric potential difference.

To achieve practical solutions from the analytical formulation described above, a FE formulation with electric potential and mechanical variables as the degrees of freedom is introduced. In the present work a eight-node 'HOD-layerwise' rectangular plate element has been developed. Although the FE implementation shown below appears standard, there is novelty in the specific form of the combination of the HOD-layerwise concept.

The real displacement functions (Eq. (1)) and strains (Eq. (3)) in terms of the nodal variables $[u_e]$ are given in Eqs. (10) and (11).

$$\begin{bmatrix} U(x,y,z)\\ V(x,y,z)\\ W(x,y,z)\end{bmatrix} = [A(z)][N_u(\xi,\eta)][u_e] \tag{10}$$

$$\begin{aligned}[\varepsilon_b(x,y,z)] &= [D_b(x,y,z)][N_u(\xi,\eta)][u_e]\\ [\varepsilon_s(x,y,z)] &= [D_s(x,y,z)] + [N_u(\xi,\eta)][u_e]\end{aligned} \tag{11}$$

The shape function matrix $N_u(\xi,\eta)$ in Eq. (10) is an $11 \times (11 \times 8)$ matrix that uses the standard eight-node serendipity shape functions. The electric counterpart of the shape function matrix is, $N_\phi(\xi,\eta,z)_k$, with dimension $1 \times 8(n+1)$ and it incorporates the layerwise and the eight-node shape functions. It relates the nodal voltages to the voltage function (Eq. (12)) of the eth element at the kth layer and the electric field (Eq. (13)).

$$\Phi(x,y,z)_k^e = [N_\phi(\xi,\eta,z)_k][\phi_e] \tag{12}$$

$$[E(x,y,z)]_k^e = -\nabla[N_\phi(\xi,\eta,z)_k][\phi_e] \tag{13}$$

where $\nabla =$ the gradient operator.

Finally, applying the variational principle by including the definitions of Eqs. (10)–(13) the governing equation of the structure in terms of the FE nodal variables is obtained in Eq. (14).

$$\begin{bmatrix} [K_{uu}] & [K_{u\phi}] \\ [K_{\phi u}] & [K_{\phi\phi}] \end{bmatrix} \begin{bmatrix} u_g \\ \phi_g \end{bmatrix} = \begin{bmatrix} [F_g] \\ -[Q_g] \end{bmatrix} \tag{14}$$

Eq. (14) represents the summation of the equations of all the elements and thus is the global equation for the system, hence the subscripts 'g'. This formulation is general in the sense that it can model laminated composite structures with arbitrary boundary conditions. The robustness of this formulation is that each element of each layer can be made of any material and if it is piezoelectric, then setting the appropriate (electrical) boundary conditions will allow it to act as an actuator or sensor. The element is validated by comparing to known elements and results (Chee et al., 2000a,b).

3. Multi-criteria shape control

As mentioned in the Introduction, this paper will focus on dual-criteria shape control where the transverse displacements and curvatures are used to measure the conformity with the desired shape. The use of displacements and slopes had been presented in Chee et al. (2000c).

3.1. Defining the problem

The structure whose shape is to be controlled is a laminated composite plate where the piezoelectric actuators can be embedded or surface attached. The electric field is applied in the normal direction of the composite plane. The actuators are discretized as "patches" to distinguish them from the hypothetical-computational "elements" in FEA. Thus, for the FEA, a patch is constructed of at least one finite element. The size of the patch is the real size of the actuator while the size of the element is determined by the user depending on the structural topology and desired accuracy of the FE mesh. The top and bottom surfaces of each patch have constant voltages.

The shape control problem analyzed in this paper involves finding the voltage distribution, that is, the magnitude of voltages to be applied to each of the piezoelectric patches. The desired shape of the structure is known, either as a mathematical function or the specification of the displacements at the nodes. There exists a linear relationship between the voltage and displacement (Chee et al., 2000b) and hence also between the voltage and curvatures due to the linear model of the constitutive properties and the governing equations. Thus the curvatures (for the eth element) and transverse nodal displacements (for the whole structure) can be directly related to the applied patch voltages (Eqs. (15) and (16)) by the influence coefficient matrices obtained by FEA.

$$\{w\} = [C_w]\{\phi\} = \sum_{k=1}^{N_p} \{C_w\}_k \phi_k = \{C_w\}_1 \phi_1 + \{C_w\}_2 \phi_2 + \cdots + \{C_w\}_{N_p} \phi_{N_p} \tag{15}$$

where $K_{xx} = -\partial\psi_x/\partial x$, $C_{K_{xx}} =$ matrix of coefficient of K_{xx}, $\phi_k =$ voltage on patch k, $N_p =$ number

$$\{K_{xx}\} = [C_{k_{xx}}]\{\phi\} = \sum_{k=1}^{N_p} \{C_{k_{xx}}\}_k \phi_k \tag{16}$$

of active patches.

The curvatures K_{yy} and K_{xy} are defined similarly to K_{xx}. Note that the curvatures are defined using the first order terms of the third order displacement field (Eq. (1)), in order to account for the transverse shear deformations (Koconis et al., 1994a; Kollar, 1990). When the voltage is perturbed by a small amount $\mathrm{d}\phi_k$ at patch k only, from the base voltage configuration $\{\phi^0\}$, then the curvatures of the perturbed structure is given by Eq. (17), where superscript 0 = quantities in base configuration. This concept is utilized in the development of the PBVD algorithm in the following section.

$$\{K_{xx}\} = \{K_{xx}^0\} + \{C_{K_{xx}}\}_k \,\mathrm{d}\phi_k \tag{17}$$

4. Preliminary investigation with multi-criteria linear least squares

The conformity of the actual shape with the desired shape will be measured using the sum of squared differences of the displacements, slopes and curvatures (although slopes will not be the control criteria) as defined in Eq. (18). The slopes S_x and S_y are defined in Chee et al. (2000c) while the slope measure LS S_y and the curvature measures LS K_{yy}, LS K_{xy} are defined similarly to their counterparts in Eq. (18).

$$\mathrm{LS}\, w = \sum_{i=1}^{N_n} \frac{(w_i - w_i^{\mathrm{d}})^2}{\mathrm{Max}_{\forall i}(|w_i^{\mathrm{d}}|)^2}, \quad \mathrm{LS}\, S_x = \sum_{i=1}^{N_S} \frac{(S_{x\,i} - S_{x\,i}^{\mathrm{d}})^2}{\mathrm{Max}_{\forall i}(|S_{x\,i}^{\mathrm{d}}|)^2}, \quad \mathrm{LS}\, K_{xx} = \sum_{i=1}^{N_K} \frac{(K_{xx\,i} - K_{xx\,i}^{\mathrm{d}})^2}{\mathrm{Max}_{\forall i}(|K_{xx\,i}^{\mathrm{d}}|)^2} \tag{18}$$

where N_n, N_S and N_K are the number of points where displacement, slopes and curvatures are measured; superscript d = desired variables.

Extending the well-known LLS method to the multi-criteria case (McLLS), the corresponding objective function for CDSC is given in Eq. (19).

$$\mathrm{LS\,obj} = \alpha^{w}\mathrm{LS}\, w + \alpha^{K_{xx}}\mathrm{LS}\, K_{xx} + \alpha^{K_{yy}}\mathrm{LS}\, K_{yy} + \alpha^{K_{xy}}\mathrm{LS}\, K_{xy} \tag{19}$$

The structural model for the following set of tests is depicted in Fig. 1. The 20 shaded regions represent areas designated as active patches. For the FEA, the structure is divided into 99 elements and four layers. In

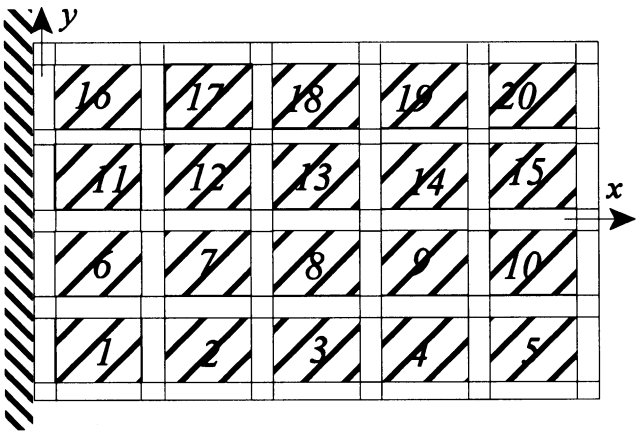

Fig. 1. Cantilever plate with 99 elements and 20 active patches (not to scale).

the present case, each patch is modeled by one finite element. The dimensions of the cantilever plate are length $(L) = 0.150$ m, width $(C) = 0.120$ m and the thickness of the single-layered substrate is 2.0×10^{-3} m. The gap between the patches and the edge are 0.005 m and the gaps between the patches themselves are 0.010 m. The Aluminum substrate has the following stiffness (GPa): $c_{11} = c_{22} = c_{33} = 105.896$, $c_{12} = c_{23} = c_{13} = 54.552$, $c_{44} = c_{55} = c_{66} = 25.67$. The piezoelectric actuators (PIC151), with thickness of 5.0×10^{-4} m, are located at the regions corresponding to the patches and are attached to the top and bottom layer of the substrate. Their properties are stiffness (GPa): $c_{11} = c_{22} = 107.6$, $c_{33} = 100.4$, $c_{12} = 63.12$, $c_{23} = c_{13} = 63.85$, $c_{44} = c_{55} = 19.62$, $c_{66} = 22.24$; electric permittivity (nF/m): $\chi_{11} = \chi_{22} = 9.818$, $\chi_{33} = 7.536$; piezoelectric strain constants (pm/V): $d_{31} = d_{32} = -214.0$, $d_{33} = 423.0$, $d_{15} = d_{24} = 610.0$.

The present study focuses in obtaining a *twisted* desired shape because this is the interesting case where PBVD is needed to improve the structure after the initial displacement shape control stage (Fig. 2). The desired shape is specified by Eq. (20) where G is the scaling factor, in this case $G = 1$. The twisted, wide cantilever example may represent a wing structure that is required to be twisted for aerodynamic purposes.

$$w(x,y) = \frac{(\cosh(x) - 1)\sin(y)}{G} \tag{20}$$

Recall that the aim to reduce the bumpiness of the resultant structure from DBSC (e.g. in case 1) led to the proposal of MCSC. The series of tests, described in Table 1, varies the weights for each of the criteria. In essence, cases 2–6 (Table 1) investigates the combinations of various criteria with respect to case 1 which used only displacements as the SC criterion – DBSC. The weights are limited to a value of 0 or 1. In general

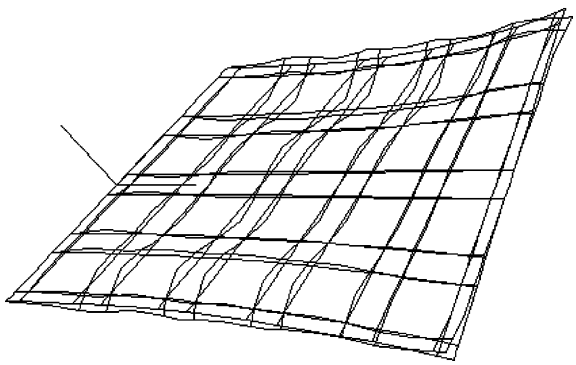

Fig. 2. Midplane transverse displacement of cantilever plate with a twisted desired shape. Actual shape by displacement LLS is superimposed (Oblique view).

Table 1
Test cases for MCSC using McLLS by variation of weights

Case	Weights				Figure
	α^W	$\alpha^{K_{xx}}$	$\alpha^{K_{yy}}$	$\alpha^{K_{xy}}$	
1	1	0	0	0	2
2	0	1	1	1	3
3	1	1	1	1	3
4	1	1	0	0	3
5	1	0	1	0	3
6	1	0	0	1	4

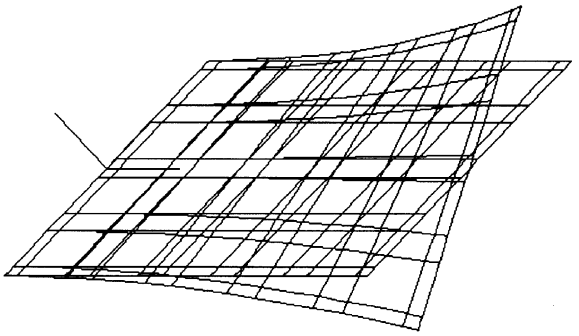

Fig. 3. Case 2 – Structure is smoothed but tip diverge excessively. Cases 2–5 have similar response.

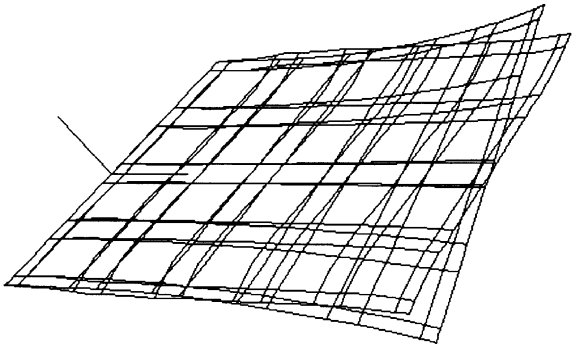

Fig. 4. Case 6 – Using w and K_{xy} criteria only. Region near wall is smoothed but tip region diverges and curls.

the weights can have any positive real value, but this test series is only interested in examining some overall major effects. The response to the different weight settings on the actual structure can be seen graphically in the oblique views in Figs. 3 and 4, where the actual shapes were superimposed on the desired shape. Note that cases 2–5 responded similarly so they are represented by Fig. 3.

Numerical results that indicate the conformity of the actual shape to the desired shape are shown in Figs. 5 and 6 which compares normalized LS displacements LS w, slopes LS S_x, LS S_y and curvatures LS K_{xx}, LS K_{yy}, LS K_{xy}, as defined in Eq. (18). Note that these six quantities are normalized further with respect to their counterparts in Case 1 – which uses the displacement criterion only. Fig. 6 is the magnified version of Fig. 5, excluding the LS w and tip displacement values which are usually much larger than 1. The following observations are made from Figs. 3–6:

(1) The inclusion of any other criteria besides displacements, increases the differences in displacements between the desired and actual shape, i.e. LS w(case i)/LS w(case 1)>1, where $i = 2, \ldots, 6$. Graphically, this can be seen in Fig. 2 as the case that uses the displacement criterion only (case 1), having the best match between actual and desired shape among the other cases, although the structure appears bumpy.

(2) In terms of matching displacements, graphically the six cases fall into three distinguishable groups. This is reflected in Fig. 5 where the LS w values for the six cases fall into three distinct ranges.

(3) Cases 2–5 (see Fig. 5) show the worst match for displacements, i.e. highest LS w values and the greatest divergence in displacement at either end of the free corners. The common feature here is the use of

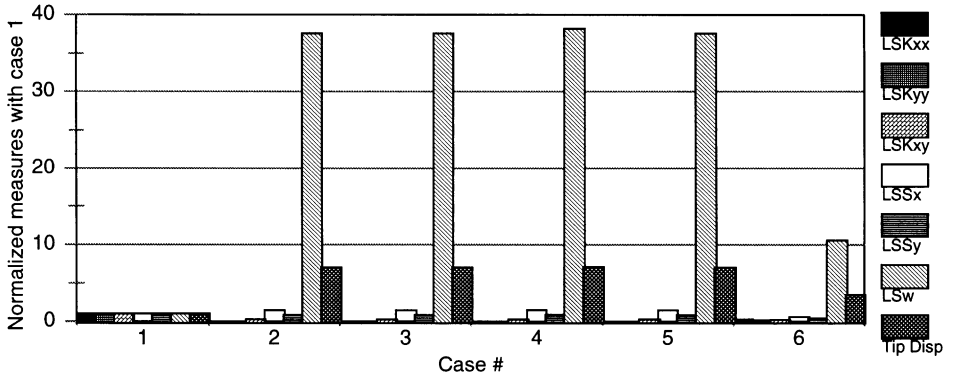

Fig. 5. Least square measures of displacement LS w, slopes LS S_x, LS S_y and curvatures LS K_{xx}, LS K_{yy}, LS K_{xy} and tip displacement at free corner for MCSC using McLLS.

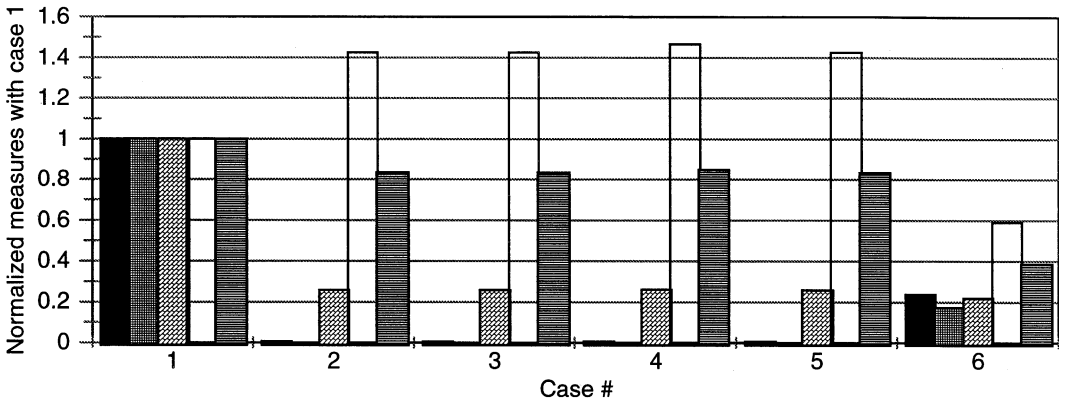

Fig. 6. Magnified version of Fig. 5 – excluding LS w and tip displacement.

either the K_{xx} or K_{yy} as the SC criteria. This infers the dominance of these two curvature criteria, meaning that if they are used as control criteria, then all other criteria have almost no influence. Thus the algorithm forces the structure to conform to the desired curvatures strongly while neglecting the other criteria. Not surprisingly for these four cases, there is drastic reduction in the LS K_{xx} and the LS K_{yy} values with respect to case 1, see Fig. 6. The slopes S_x did not perform that well either.

To summarize, curvatures tend to dominate over the displacement criteria, such that the presence of curvature criteria means it is difficult to control displacements. When the curvatures are improved (less bumpiness and lower LS values for curvatures) then the displacements, especially at the tip of the cantilever, diverges from the desired shape even more. The set of observations above is based on the structure in Fig. 1, thus the observations do not necessarily apply to all shape control problems. A few points that can be generalized are: (i) Some criteria may have strong dominance over the others. (ii) The displacement criteria may be weak, therefore while other criteria are controlled, the resultant displacements may not conform satisfactorily to the desired shape. (iii) It is impossible to improve all criteria simultaneously for all shape control problems. As a further note, the method of simulated annealing (SA) has also been used to conduct MCSC, however the results did not reveal anything extra over the observations made by McLLS. Most of the SA results indicate similar drawbacks to the McLLS method and so it is not necessary to present their results here.

In this simple series of tests, the weights are only given the values of 0 or 1 which means their corresponding criteria can either be switched on or off. In reality, there is an infinite combination of weights that are possible. Since the performance of the McLLS depends on the selection of weights, this procedure is non-trivial and it is difficult to achieve a satisfactory solution because the selection of weight is also non-intuitive. In fact there is no best result and some cases produce better conformity to the desired shape in certain criteria than others. Thus, what is needed is an algorithm that automatically reduces the bumpiness by improving the curvature criteria and yet not allowing the displacement criteria to deteriorate significantly – this is the objective of the algorithm developed in the next section, known as the PBVD.

5. Perturbation buildup voltage distribution method for shape control

Many existing shape control algorithms are formulated from displacement based cost function. Chee et al. (2000b) showed that simple desired shapes and configurations can be obtained with relative ease while more complex desired shapes or structural configurations are achievable globally but introduces some unevenness locally. However, this leads to bumpiness of the transverse displacement profile as shown in Fig. 2. Investigations using dual criteria curvature–displacement McLLS shape control (previous section) appeared to be have smoothed certain regions of the structure but tip displacements are worse than in the DBSC case. In addition, the determination of weights would not be a trivial task. Thus an iterative perturbation technique is introduced and it implicitly targets regions that need the most improvement. The PBVD concentrates on iteratively correcting the curvatures locally. A consequence of PBVD will be the smoothing of the actual structure because the curvatures are being controlled. And this is achieved without significant sacrifice of the target displacement. Although the name and concept of the algorithm is motivated by BVD – a purely DBSC method (Chee et al., 2000b) – the PBVD algorithm is significantly different.

5.1. The perturbation buildup voltage distribution algorithm

The PBVD method starts with the initial configuration which is the resultant of DBSC using LLS. The strategy involves improving the curvature of the structure on an elemental basis – where the elements with larger curvature discrepancies (compared to the desired curvature values) will be improved first. The voltage required to improve the curvatures in an element will be calculated such that only small improvements are made at each iteration, hence requiring only small amounts of incremental voltage at a time.

The measure of transverse displacements is the *sum of the squared difference* (Δw) between the desired and the actual nodal values (see Eq. (21a)). But the curvatures are measured on an elemental basis hence the *area integral of the squared difference* (ΔK^e_{xx}, ΔK^e_{yy}, ΔK^e_{xy}) of the desired and actual curvature is used (see Eq. (21b)). This has the advantage of placing more importance on the improvement of curvatures of larger sized elements.

$$\Delta w = \sum_{i=1}^{N_n} (w_i - w_i^{\mathrm{d}})^2 \tag{21a}$$

$$\Delta K^e_{xx} = \int_{A_e} (K^e_{xx} - K^{e\,\mathrm{d}}_{xx})^2 \,\mathrm{d}A_e, \quad \Delta K^e_{yy} = \int_{A_e} (K^e_{yy} - K^{e\,\mathrm{d}}_{yy})^2 \,\mathrm{d}A_e, \quad \Delta K^e_{xy} = \int_{A_e} (K^e_{xy} - K^{e\,\mathrm{d}}_{xy})^2 \,\mathrm{d}A_e \tag{21b}$$

To investigate the voltage perturbation effect on the curvature, the new curvature is compared with the original curvature with respect to the desired curvature. Since the displacement and curvature are in fact competing criteria, the improvement of the curvature of the structure will be at the expense of achieving the

desired displacement, as shown using the McLLS in the previous section. By incorporating a tolerance factor p, it is possible to aim for an improvement in the curvature at the same time as restricting the displacement criteria from deteriorating excessively. This dual criteria is expressed in Eq. (22).

$$\begin{aligned}&\int_A (K^e_{xx} - K^{e\,\mathrm{d}}_{xx})^2\,\mathrm{d}A_\mathrm{e} < (1-p)\int_A (K^{e\,0}_{xx} - K^{e\,\mathrm{d}}_{xx})^2\,\mathrm{d}A_\mathrm{e}\\ &\sum_{i=1}^{\text{nodes}} (w_i - w_i^\mathrm{d})^2 < (1+p)\sum_{1}^{\text{nodes}} (w_i^0 - w_i^\mathrm{d})^2\end{aligned} \tag{22}$$

where superscript d = desired quantities. Note that the equations involving K_{yy} and K_{xy} would be similar to Eq. (22).

During each iteration, an incremental voltage will be added temporarily and the effects on the curvature of the other elements as well as displacements are checked. If the side effects of adding $\mathrm{d}\phi$ are tolerable, then it is added permanently and the new voltage configuration will be used in the next iteration.

Perturbing the voltage at the kth patch only, the dual criteria is re-expressed as Eq. (23) and enable the calculation of the optimum incremental voltage $\mathrm{d}\phi$. Note that the equations involving K_{yy} and K_{xy} are similar to Eq. (23) but not shown here. The algorithm will choose the element and the *type* of curvature, which needs the most improvement, to act upon.

$$\begin{aligned}&p\int (K^{e'}_{xx})^2\,\mathrm{d}A + 2\mathrm{d}\phi\int (K^{e'}_{xx})(C^e_{K_{xx}})_k\,\mathrm{d}A + \mathrm{d}\phi^2\int (C^e_{K_{xx}})^2_k\,\mathrm{d}A < 0\\ &-p\sum_{i=1}^{\text{nodes}} (w'_i)^2 + 2\mathrm{d}\phi\sum_{i=1}^{\text{nodes}} w'_i (C^e_w)_{ki} + \mathrm{d}\phi^2\sum_{i=1}^{\text{nodes}} (C^e_w)^2_{ki} < 0\end{aligned} \tag{23}$$

where $K^{e'}_{xx} = K^{e\,0}_{xx} + K^{e\,\mathrm{d}}_{xx}$ and $w' = w^0 + w^\mathrm{d}$.

Another quantity that is used later is the CPI and is defined in Eq. (24).

$$\begin{aligned}&\mathrm{CPI}^{K_{xx}}(k,e) = \frac{\phi_k - \phi_k^0}{\Delta K^e_{xx} - \Delta K^{e\,0}_{xx}}, \quad \text{with} \quad \phi_k = \phi_k^0 + \mathrm{d}\phi \ \text{ and } \ \mathrm{d}\phi = 1.0\\ &\mathrm{CPI}^{K_{xx}}(k,e) = \frac{1}{\int_{A_e} C^e_{K_{xx_k}}(C^e_{K_{xx_k}} + 2K^{e'}_{xx})\,\mathrm{d}A_e}\end{aligned} \tag{24}$$

Large CPI(k,e) values implies that element e is insensitive to the voltage applied to patch k.

The PBVD algorithm is summarized as follows:

1. Perform displacement shape control using LLS and use the resultant voltage configuration as the initial configuration for PBVD.
2. Calculate w_Δ and ΔK^e_{xx}, ΔK^e_{yy}, ΔK^e_{xy} for all elements e.
3. Sort the ΔK^e_{xx}, ΔK^e_{yy}, ΔK^e_{xy} from the highest magnitude to the lowest.
4. Select an element with high (ΔK^e) to be improved upon. A normal probability distribution selection mechanism is used so that elements with higher (but not necessarily the highest) (ΔK^e) magnitude are more likely to be selected.
5. Calculate $\mathrm{CPI}^{K_{xx}}(k,e)$, $\mathrm{CPI}^{K_{yy}}(k,e)$ and $\mathrm{CPI}^{K_{xy}}(k,e)$ for the kth patch and the eth element for all patches and all elements.
6. Sort the curvature sensitivities among all patches, for the selected element.
7. Begin iteration of voltage perturbation starting from the most sensitive patch.
8. Calculate incremental voltage $\mathrm{d}\phi$ necessary to improve curvature for this element but with a tolerable worsening in displacement. This is done by finding the optimum $\mathrm{d}\phi$ of Eq. (19).
9. Apply $\mathrm{d}\phi$ and recalculate Δw and ΔK^e_{xx}, ΔK^e_{yy}, ΔK^e_{xy} for all elements.

10. Check for adverse effects in the slopes of other elements when $d\phi$ was applied to patch k. If the slope of the other elements are within a tolerable limit (s tolerance factor) then accept the new voltage configuration and begin the next iteration in step 2. Otherwise, go to step 7 to perturb the next patch.
11. Continue iteration until maximum number of iterations is reached or tolerance on original Δw is exceeded.

6. Performance of perturbation buildup voltage distribution in curvature displacement shape control

A set of tests is performed here to illustrate the performance of using curvature as the perturbing criteria. The same structural model (Fig. 1) and twisted desired shape (Eq. (20)) is used as before. The voltage configuration is initialized by first using the LLS method to perform shape control with the displacement criteria only. The resulting voltage configuration is perturbed in order to improve the curvature difference between the desired and the actual shape. Various parameters of the PBVD were varied and a selection of cases representing a wide range of the results is presented here. Table 2 shows the main parameters of PBVD while Fig. 7 shows the LS measures for displacements, slopes and curvatures normalized with case 1 – where only displacement criterion is used. The LS values measure the differences, of the respective quantities, between the desired shape and the actual shape.

Table 2
Parameters for several case of CDSC using PBVD

Parameters	Case								
	1 (Ref.)	2	3	4	5	6	7	8	9
LS d tolerance	–	5.5	0.05	0.5	5.5	5.5	5.5	0.5	0.5
Mult. iter.	–	0.5	0.5	0.5	100.9	100.9	1.9	1.9	1.9
p tolerance	–	0.01	0.01	0.01	0.01	0.1	0.001	0.001	0.1
s tolerance	–	2.3	2.3	2.3	2.3	0.01	0.3	0.01	0.0001

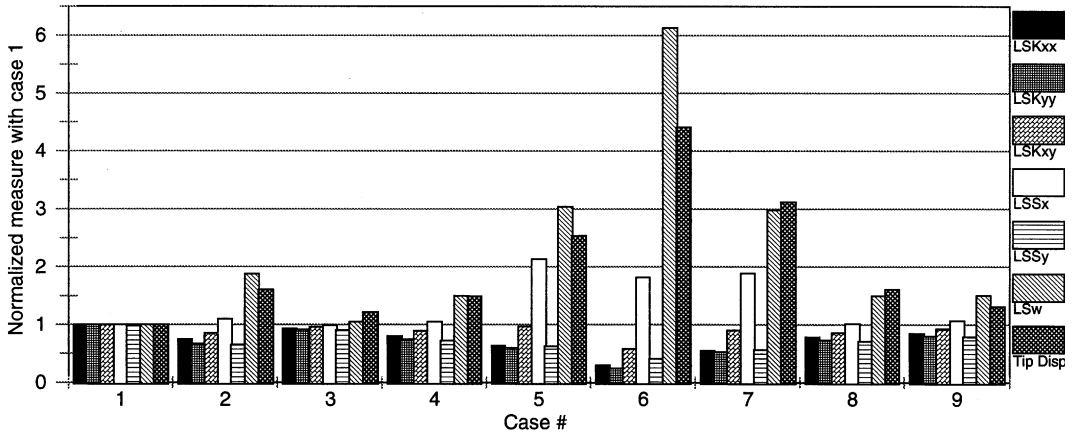

Fig. 7. Least square measures of displacement LS w, slopes LS S_x, LS S_y and curvatures LS K_{xx}, LS K_{yy}, LS K_{xy} and tip displacement at free corner for CDSC using PBVD.

It is quite clear from Fig. 7 that using PBVD in CDSC has improved the conformity of all three types of curvatures between the desired and the actual shape – i.e. normalized LS K_{xx}, LS K_{yy} and LS K_{xy} values less than 1.0. Hence a quick conclusion is that PBVD has achieved its aim in CDSC by reducing the differences between the curvatures of the desired and actual shape. This in turn has reduced the bumpiness of the structure. However, the problem is more interesting and challenging because tailoring the voltage configuration to minimize curvature difference (or slope difference in SDSC), is at the expense of the conformity of transverse displacements. When there is a good curvature match, the displacement match becomes poorer.

Hence a balance is sought between the requirements of a good displacement match and a good curvature match (reducing bumpiness). This is achieved readily by PBVD via parameters such as LS d – the tolerance of displacement deterioration or p – the tolerance associated with the size of the voltage perturbation. Thus notice in Fig. 7 that cases with very low LS curvature values (cases 5–7) also have quite large LS displacement values. In fact case 6 would suitable when there is a strong need to conform to the desired curvatures because LS K_{xx}, LS K_{yy}, LS K_{xy} and LS S_y have improved by 70%, 75%, 40% and 60% respectively; at the expense of LS w and tip displacements increasing by six and four times respectively. On the other hand cases 2, 4, 8, 9 which have moderately low LS curvature values, have LS w values which are not too excessive. Note that for this particular test model, improving the curvatures tend to improve the S_y slope but the S_x slope deteriorates a little.

The parameter *Mult. Iter.* in Table 2 is the number of inactive iterations before the algorithm terminates and is similar to a convergence parameter. In cases 5–7 where the total displacement tolerance, LS d, and Mult. Iter. is quite high, it allows the PBVD process to tolerate a greater deterioration of the displacement measure while improving the curvature. In case 2 however, although LS d is large, Mult. Iter. has a low value, thus the algorithm stops at quite low LS w value with good improvement in curvatures obtained. Restricting cases 4,8,9 to have low displacement tolerance LS d values, their LS w values are never excessively high but yet they can still achieve significant improvement in curvatures. Case 3 has a very strict LS d value thus the improvement in curvature is also quite restricted. The tip displacement at one end of the cantilever plate, see Fig. 7, is also strongly correlated with the displacement measure LS w.

Besides looking at the LS curvature values, the reduction in bumpiness can also be seen graphically. The oblique view of the transverse displacement plots of cases 4 and 7 are shown in Figs. 8 and 9 respectively. Comparing to the pure displacement control case in Fig. 2, much of the region which appear uneven or bumpy especially near the edges, have been reduced in Figs. 8 and 9 except for the central region. Also note that case 7 (Fig. 9) has a more relaxed displacement tolerance than case 4 (Fig. 8), thus the former is able to improve its curvatures to a greater extent but also notice that its tip displacement has diverged more than the latter.

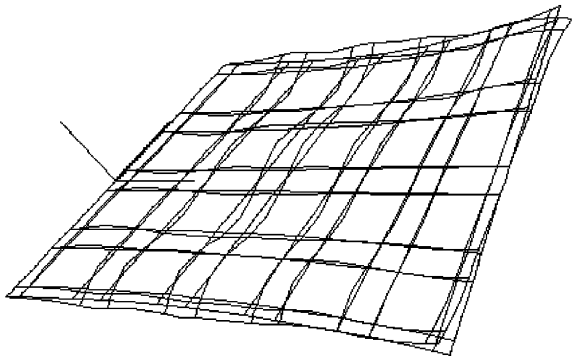

Fig. 8. Cantilever plate after PBVD procedure for CDSC, case 4. Oblique full field view of the transverse displacement.

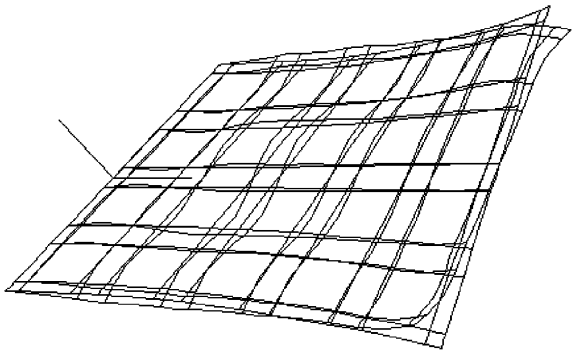

Fig. 9. Cantilever plate after PBVD procedure for CDSC, case 7. Oblique full field view of the transverse displacement.

The voltage distribution of a selected number of cases is shown in Table 3. Note that the magnitude of the voltages are quite high because of the required shape that was specified – from the desired shape Eq. (20), this amount to a maximum corner displacement of 1.35 mm. The results seem sensible since the predicted voltages does reflect an anti-symmetric pattern in order to achieve the anti-symmetric twisted shape.

From the series of tests, it was noted that the LS d is one of the important parameters and it determines the extent to which the curvatures can be improved as well as how much the displacement measure is allowed to deteriorate. The other important parameter is the p tolerance which controls the degree of perturbation at each iteration. It was found that a low value, for this case 0.001–0.01, gave reasonable results.

Table 3
Selected voltage distribution for actuator patches of cases in Table 2

Patch voltage	Cases		
	1	4	7
1	6023.5	6023.5	4886.7
2	12 126.2	10 026.7	5509.3
3	8300.9	5252.6	5101.0
4	7725.5	7451.0	3833.9
5	−3252.0	−3252.0	−7162.5
6	8596.0	8596.0	7925.8
7	−7025.2	−7025.2	−7025.2
8	−3957.5	−3957.5	−3957.5
9	−2832.5	−2832.5	−3108.9
10	−807.6	−807.6	−807.6
11	−8596.0	−8596.0	−8004.0
12	7025.2	7025.2	7025.2
13	3957.5	3957.5	3957.5
14	2832.5	2832.5	2832.5
15	807.6	807.6	807.6
16	−6023.5	−6023.5	−4630.6
17	−12 126.2	−9937.8	−5557.8
18	−8300.9	−5376.2	−5094.1
19	−7725.5	−7437.8	−4433.8
20	3252.0	3252.0	7197.1

A low value of p means that perturbation occurred slowly with fine steps, whereas high p values indicate coarser perturbation steps and may lead to poorer results. Thus the operation of this parameter is quite similar to the *cooling rate* parameter in SA which controls the quality of the solution. For this example, Mult. Iter. may be taken as 2.0 or above to prevent premature termination of the algorithm while the s tolerance, which essentially controls the side effects of perturbing an element, may be taken as 0.01. There is a degree of flexibility in choosing the last two parameters within a certain range.

The two figures of Figs. 10 and 11 are the normalized curvature and slope measures taken along the x-axis at $y = 4.5 \times 10^{-2}$ m. Cases 7–9 are omitted from the graphs because they are quite similar to cases 2, 3 and 5 respectively. The measure for the K_{yy} graph is shown here because among all three curvatures that can be improved by PBVD–CDSC, K_{yy} is the curvature that required the most improvement and therefore the PBVD algorithm automatically focuses more effort in improving this criteria. One of the positive side effects illustrated here is that using PBVD to improve the curvature will also result in an improvement of the S_y slope. However, Fig. 11 shows the conformity of the S_y slope to the desired slope deteriorates considerably near the free end of the cantilever plate for cases 5 and 6. This is not unexpected since cases 5 and 6 were specified to have a higher tolerance of displacement deterioration – this is also reflected in high LS w values in Fig. 7.

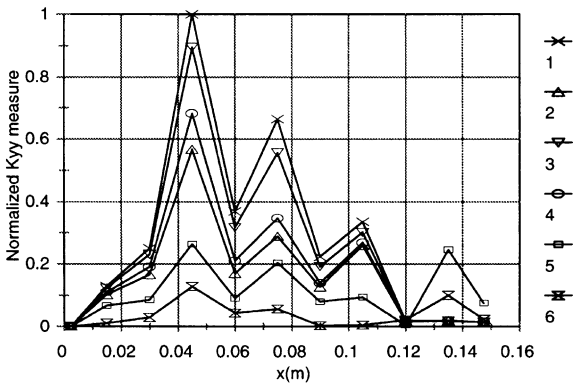

Fig. 10. Normalized curvature measure for K_{yy} for five cases of PBVD–CDSC and a reference case.

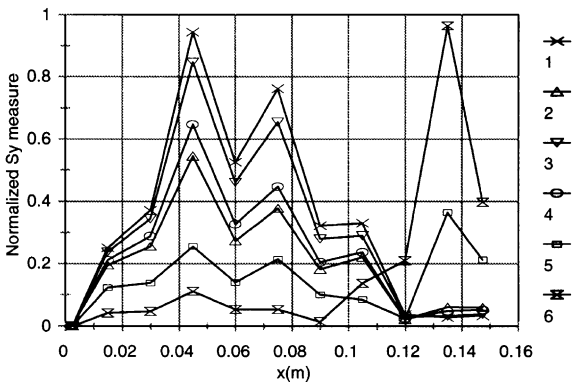

Fig. 11. Normalized slope measure for S_y for five cases of PBVD–CDSC and a reference case.

The main features of Figs. 10 and 11 illustrates that PBVD has achieved reduction in curvature, and in addition the slope S_y, when compared to reference case 1 which uses only displacements for SC. Most cases show that the curvature K_{yy} conforms better (lower values of LS K_{yy}) to its desired counterpart. The question as to which of the cases are better depends partly on the user and its application as to the importance of conformity of the curvature versus displacements.

7. Stress reduction effect

The existence of complex stress fields within a smart structure should be expected because of the independent localized actuators distributed throughout the structure. The greater number of independent active patches, the greater is the shape controllability. This is analogous to providing the structure with enough actuation degrees of freedom in order to achieve a complex shape which can be thought of as a combination of basic shapes. By imposing voltages on the actuators, the structure is being coerced into the desired shape. This effect is more forceful in the LLS method because it is a direct approach whereas the iterative approach of PBVD is more relaxed in its process of calculating the voltage distribution. In either case, when significantly different voltages are applied to various patches, as directed by the shape control algorithm, localized internal stresses are setup. This issue is particularly significant to smart structures where the actuators are not external but are regarded as an integral part of the structure.

The bumpiness of the shape of the structure is in fact changes in slope in localized regions. This means the local curvature has a higher than usual magnitude. In practical terms, this translates to high stresses in certain regions as well as large variation in stresses between other regions. Since the PBVD algorithm has the ability to smoothen the structure, it can be regarded as a secondary procedure in shape control to reduce internal structural stress caused by the primary stage which is pure displacement shape control. This conjecture has been validated by Chee et al. (2000c) for SDSC and will now be validated in CDSC using the PBVD algorithm.

The following tests (Figs. 12–15) compare the internal stresses generated within the structure as a result of the pure displacement shape control using LLS and the stresses obtained after the PBVD procedure is applied. This particular configuration from which the stresses are measured, corresponds to case 6 in Table 2. It was selected because it produced the most improvement in curvature and slope conformity, see Fig. 7. Hence it is expected to produce significant reduction in stresses. The stresses for each element are calculated

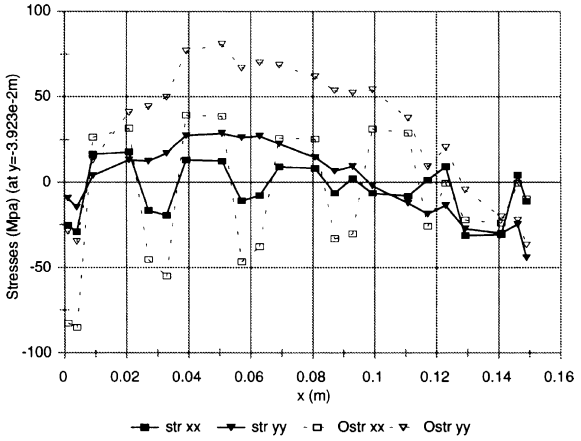

Fig. 12. Reduction of the normal in-plane stresses by the PBVD–CSDSC procedure (y-section).

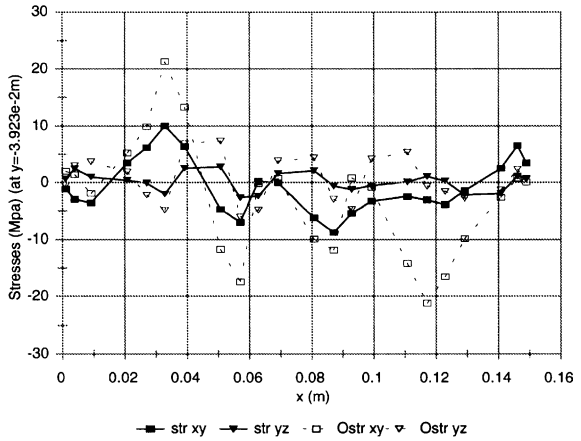

Fig. 13. Reduction of a transverse and in-plane shear stress by the PBVD–CDSC procedure (y-section).

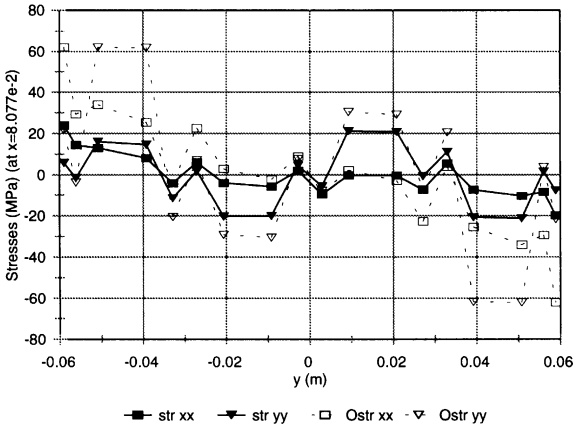

Fig. 14. Reduction of the normal in-plane stresses by the PBVD–CDSC procedure (x-section).

at their 2×2 Gauss points at a height of $z = 9.0 \times 10^{-4}$ m, which is within the Aluminum substrate. Although all six stresses were calculated, only a selection of the results are presented here due to space limitation. The normal in-plane stresses at $y = -3.923 \times 10^{-2}$ m along the length of the structure is shown in Fig. 12 – dashed lines for stresses without PBVD and solid lines for stresses with PBVD. There is a clear reduction in the axial stress σ_y along the entire length of the structure and it is mainly tensile stresses. Several points with high σ_x magnitudes were also reduced significantly and also note that this stress is compressive in some regions and tensile in others.

The in-plane shear stress (τ_{xy}) and one of the transverse shear stresses (τ_{yz}) are plotted in Fig. 13 at $y = -3.923 \times 10^{-2}$ m. Although the transverse shear stress may be smaller in magnitude compared to the other stresses, it is clearly not negligible. This justifies the need to use a displacement field such as the present one that is able to capture the transverse shear effects. From Fig. 13 it can be seen that at points with high stress magnitudes, applying PBVD would reduce their magnitudes significantly. This effect is consistent with the PBVD algorithm which was founded on the premise of reducing the worst local effects.

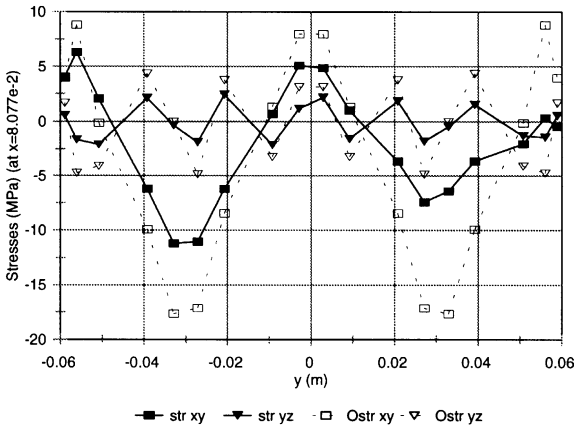

Fig. 15. Reduction of a transverse and in-plane shear stress by the PBVD–CDSC procedure (x-section).

The normal in-plane stresses at the perpendicular cross-section, $x = 8.077 \times 10^{-2}$ m is plotted in Fig. 14 while the transverse and in-plane shear stresses are found in Fig. 15. This cross-section is almost at the center of the cantilever plate running across its width. Regions of high stresses in both Figs. 14 and 15 has been significantly reduced. For example in Fig. 14, the maximum reduction of σ_{yy} of approximately 60–16 MPa (73%) was achieved, while in Fig. 13 the in-plane shear (twist) stress τ_{xy} was reduced from 22 to 5 MPa (77%) at one region. Note that in all graphs, the discrete nature of the stress distribution is quite evident and this is a mere reflection of the discrete actuator patch layout of the physical structure.

Comparison of the stresses obtained by the current CDSC process with its counterparts using the SDSC process (Chee et al., 2000c) shows a greater reduction in stresses for the former case. The reason is because CDSC focus on improving the curvature conformity with the desired shape, although the slope conformity does improve alongside, and vice versa for SDSC. Hence as the curvature criteria improves to a greater extent in CDSC, the stress reduction is also greater since curvature is proportional to stress in classical mechanics.

The graphs of Figs. 12–15 gives an indication of the magnitude of stress reduction at certain cross-sections. The discreteness of the actuator patches have considerable effects on the entire stress field as indicated by the abrupt changes in magnitudes over the domain of the structure. The complexity of the stress fields is more readily appreciated by looking at the full field view of the stress field as shown in Figs. 16 and 17. The two pairs of plots in Figs. 16 and 17 represent the σ_{xx} axial stress components and the τ_{zx} transverse shear stress (in Pa), and each pair compare the stresses that results from DBSC using LLS and the additional process of CDSC using PBVD. There are regions in which stresses have reduced quite substantially and there does not appear to be any observable increase in stresses in other regions. In essence, the PBVD for the CDSC process does not only calculate the voltages required to manipulate the structure into a desired shape, it also ensures that its voltage configuration will generate less stresses compared to the case when only the displacement criterion is used.

8. Conclusion

A novel shape control algorithm that uses both displacement and curvature criteria is presented here. The FE formulation was based on a combination of third order displacement field and layerwise concept

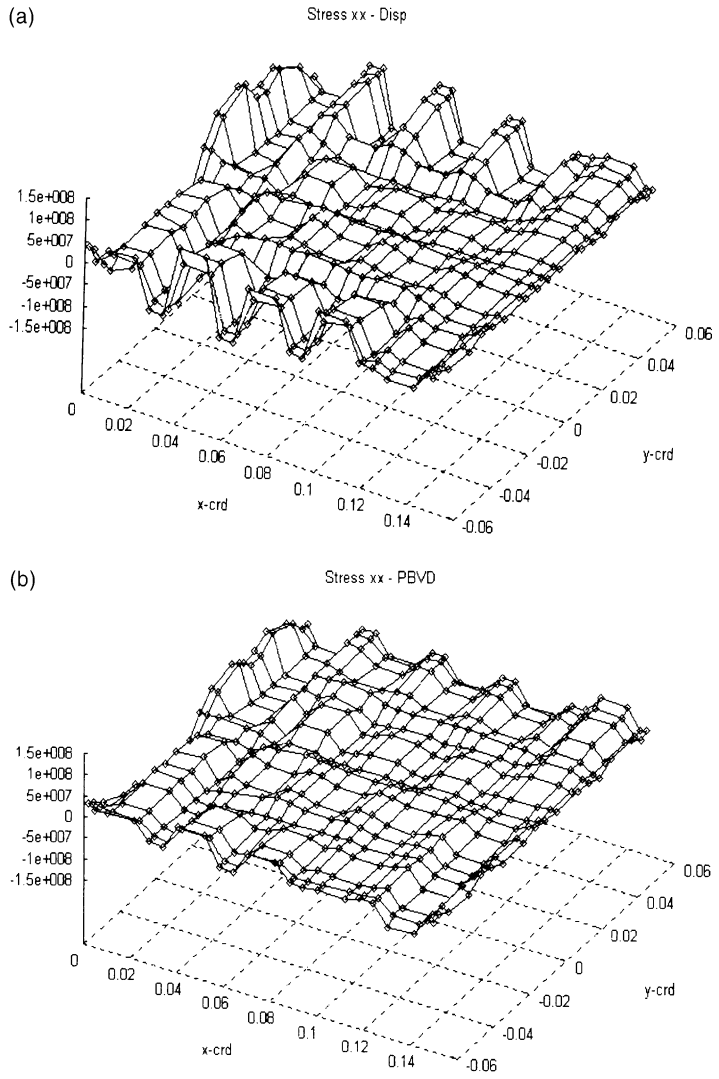

Fig. 16. (a) Pure displacement control – Stress *xx*. (b) CDSC with PBVD – Stress *xx*.

developed by the authors for laminated smart composite plate structures. Many existing shape control algorithms are displacement based which yield reasonable results. However for an extended structure with many independent actuators distributed across the structure, it was found that pure DBSC predicts a voltage configuration which when applied, produces regions of bumpiness in the shape due to localized effects. The PBVD is an iterative algorithm designed to reduce this effect by targeting some of the worst effected regions by using curvature values. Regions where the desired curvature differs most from the actual curvature are improved first. Since the displacement and curvatures are conflicting criteria, the curvatures would have to be improved at the expense of the displacement. This has been designed into the algorithm to enable the user to decide the extent of the worsening of the displacement criteria that is tolerable. The results have shown that the algorithm is successful in achieving its goal of determining the voltage con-

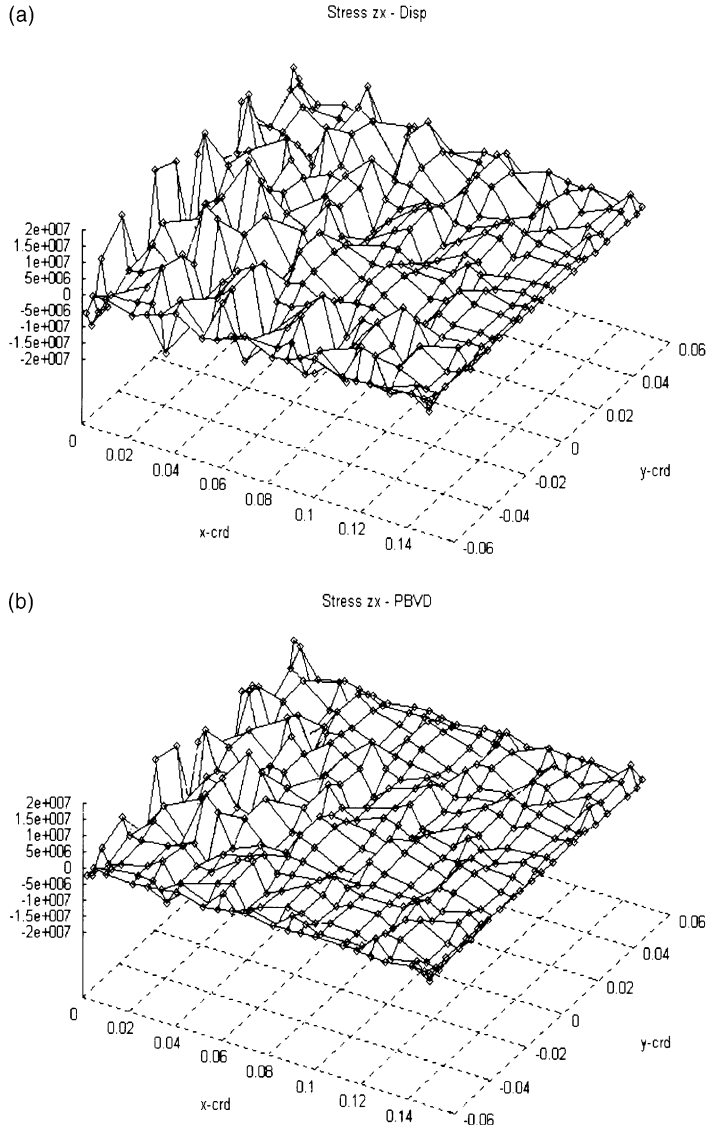

Fig. 17. (a) Pure displacement control – Stress zx. (b) CDSC with PBVD – Stress zx.

figuration to actuate the structure to conform to the desired shape and smoothing the structure to a certain extent.

In addition to smoothing the actual structure's shape, a more practical advantage of this application is that it produces less internal stresses than using DBSC. In real structures where discrete actuators are in operation, although the bumpiness may not always be obvious, the large gradients imply large internal strains and thus large internal stresses. Thus the significance of smoothing extends to alleviating unnecessary internal stresses that could be generated if a purely displacement shape control is used. This prevents over-stressing of the structure and reduce chances of de-bonding in composites applications. Results show that PBVD preferentially reduces the high magnitude stresses to a greater extent than others – especially high stress peaks.

It is worth pointing out that the proposed method and concept can be readily adapted to the problem of optimal actuator layout in an active structure.

Acknowledgements

The authors acknowledge the support of the Australian Research Council under the large grant scheme (Grant no. A89905990). C. Chee is a recipient of the APA postgraduate award and the Aeronautical Engineering Department Supplementary Scholarship.

References

Balakrishnan, A.V., 1994. Shape control of plates with piezo actuators and collocated position/rate sensors. Applied Mathematics and Computation 63, 213–234.

Chandrashekhara, K., Varadarajan, S., 1997. Adaptive shape control of composite beams with piezoelectric actuators. Journal of Intelligent Material Systems and Structures 8 (2), 112–124.

Chee, C., Tong, L., Steven, G., 2000a. A mixed model for adaptive composite plates with piezoelectric for anisotropic actuation. Computers and Structures 77 (3), 253–268.

Chee, C., Tong, L., Steven, G., 2000b. A buildup voltage distribution (BVD) algorithm for shape control of smart plate structures. Computational Mechanics 26 (2), 115–128.

Chee, C., Tong, L., Steven, G., 2000c. Static shape control of composite plates using a slope–displacement based algorithm. 41st AIAA/ASME/ASCE/AHS/ASC Structures, Structural Dynamics, and Materials Conference, Atlanta, Georgia, USA, 3–7 April, 2000.

Donthireddy, P., Chandrashekhara, K., 1996. Modelling and shape control of composite beams with embedded piezoelectric actuators. Composite Structures 35 (2), 237–244.

Eisenberger, M., Abramovich, H., 1997. Shape control of non-symmetric piezolaminated composite beams. Composite Structures 38 (1–4), 565–571.

Haftka, R.T., Adelman, H.M., 1985. Selection of actuator locations for static shape control of large space structures by heuristic integer programming. Computers and Structures 20 (1–3), 575–585.

Hsu, C.Y., Lin, C.C., Gaul, L., 1997. Shape control of composite plates by bonded actuators with high performance configuration. Journal of Reinforced Plastics and Composites 16 (18), 1692–1710.

Koconis, D.B., Kollar, L.P., Springer, G.S., 1994a. Shape control of composite plates and shells with embedded actuators. I. voltages specified. Journal of Composite Materials 28 (5), 415–458.

Koconis, D.B., Kollar, L.P., Springer, G.S., 1994b. Shape control of composite plates and shells with embedded actuators. II. desired shape specified. Journal of Composite Materials 28 (3), 262–285.

Kollar, L., 1990. Buckling of generally anisotropic shallow sandwich shells. Journal of Reinforced Plastics and Composites 9, 549–568.

Lo, K.H., Christensen, R.M., Wu, E.M., 1977. A high order theory of plate deformation-Part 1 and 2: homogeneous plates. Journal of Applied Mechanics 44, 663–676.

Okubo, H., Komatsu, N., Tsumura, T., 1996. Tendon control system for active shape control of flexible space structures. Journal of Intelligent Material Systems and Structures 7 (4), 470–475.

Paradies, R., Hertwig, M., Elspass, W.J., 1996. Shape control of an adaptive mirror at different angles of inclination. Journal of Intelligent Material Systems and Structures 7 (2), 203–210.

Reddy, J.N., 1984. A simple higher order theory for laminated composite plates. Journal of Applied Mechanics 51, 745–752.

Robbins, D.H., Reddy, J.N., 1991. Analysis of piezoelectrically actuated beams using a layer-wise displacement theory. Computers and Structures 41, 265–279.

Saravanos, D.A., Heyliger, P.R., 1995. Coupled layerwise analysis of composite beams with embedded piezoelectric sensors and actuators. Journal of Intelligent Material Systems and Structures 6, 350–363.

Subramanian, G., Mohan, P., 1996. A fast algorithm for the static shape control of flexible structures. Computers and Structures 59 (3), 485–488.

Tabata, M., Natori, M.C., 1996. Active shape control of a deployable space antenna reflector. Journal of Intelligent Material Systems and Structures 7 (2), 235–240.

Tan, Z., Bainum, P.M., 1994a. Optimal linear quadratic gaussian digital control of an orbiting tethered antenna/reflector system. Journal of Guidance, Control and Dynamics 17 (2), 234–241.

Tan, Z., Bainum, P.M., 1994b. The hybrid control of an orbiting tethered antenna/reflector system. Journal of Astronautical Sciences 42 (3), 343–359.

Tiersten, H.F., 1969. Linear Piezoelectric Plate Vibrations – Elements of the Linear Theory of Piezoelectricity and the Vibrations of Piezoelectric Plates, Plenum Press, New York.

Varadarajan, S., Chandrashekhara, K., Agarwal, S., 1998. Adaptive shape control of laminated composite plates using piezoelectric materials. AIAA Journal 36 (9), 1694–1698.